

The dynamical playground of a higher-order nonlinear Schrödinger equation: from orbital connections and limit cycles to invariant tori and the onset of chaos

V. Achilleos,¹ A. R. Bishop,² S. Diamantidis,³ D. J. Frantzeskakis,⁴
T. P. Horikis,⁵ N. I. Karachalios,³ and P. G. Kevrekidis^{6,2}

¹*Laboratoire d'Acoustique de l'Université du Maine, Avenue O. Messiaen 72085, Le Mans, France*

²*Center for Nonlinear Studies and Theoretical Division,*

Los Alamos National Laboratory, Los Alamos, New Mexico 87545, USA

³*Department of Mathematics, University of the Aegean, Karlovassi, 83200 Samos, Greece*

⁴*Department of Physics, University of Athens, Panepistimiopolis, Zografos, Athens 15784, Greece*

⁵*Department of Mathematics, University of Ioannina, Ioannina 45110, Greece*

⁶*Department of Mathematics and Statistics, University of Massachusetts, Amherst MA 01003-4515, USA*

The dynamical behavior of a higher-order nonlinear Schrödinger equation is found to include a very wide range of scenarios due to the interplay of higher-order physically relevant terms. The dynamics extends from Poincaré-Bendixson-type scenarios, in the sense that bounded solutions may converge either to distinct equilibria via orbital connections, or space-time periodic solutions, to the emergence of almost periodic and chaotic behavior. Suitable low-dimensional phase space diagnostics are developed and are used to illustrate the different possibilities and to identify their respective parametric intervals.

PACS numbers: 02.30.Jr, 05.45.-a

The nonlinear Schrödinger equation (NLS) is often associated with the theory of solitons and integrable systems [1]. In its standard form, it constitutes one of the universal nonlinear evolution equations, with applications ranging from water waves to optics, and has received enormous attention. Remarkable phenomena are also exhibited by its higher-order variants, emerging in a diverse spectrum of applications such as nonlinear optics [2] and Bose-Einstein condensates [3]. An example of this type arises when such an infinite dimensional system is found to exhibit (and potentially be attracted to) low-dimensional dynamical features, such as: (a) one or more equilibria (and orbits connecting them), (b) periodic orbits, (c) quasi-periodic orbits or (d) low-dimensional chaotic dynamics [4].

The availability of the dynamical scenarios (a)-(d) depends on the effective dimensionality of the low dimensional behavior; one-dimensionality only allows fixed points, planar systems governed by the Poincaré-Bendixson (PB) theorem [4] can also feature periodic orbits, while higher dimensions allow for quasi-periodic or chaotic dynamics. Various prototypical partial differential equation (PDE) models have demonstrated a PB-type behavior as an intermediate bifurcation stage for the route to spatiotemporal chaos. Examples include the Kuramoto-Sivashinsky [5] and complex Ginzburg-Landau [6] equations. In addition to the above autonomous systems, spatiotemporal chaos was also found in non-autonomous ones, due to the interplay between loss and external forces, such as damped-driven NLS [7–9] (where the hyperbolic structure of the underlying integrable NLS is a prerequisite [10]) and sine-Gordon [11] models.

In this work we reveal the existence of all the above prototypical examples of low-dimensional dynamics in an autonomous, physically relevant higher-order NLS

model. In particular, we show that, varying specific terms, a transition path can be traced from dynamics reminiscent of PB, including orbital connections between steady states of high multiplicity and convergence to limit cycles, to invariant tori or even chaotic attractors. Our model is the NLS equation:

$$\partial_t u + \frac{is}{2} \partial_x^2 u - i|u|^2 u = \gamma u + \delta |u|^2 u + \mu \partial_x (|u|^2 u) + \beta \partial_x^3 u + (\nu - i\sigma_R) u \partial_x (|u|^2), \quad (1)$$

where $u(x, t)$ is a complex field, γ , δ , σ_R and μ , ν are real constants, while $s = \pm 1$ denotes normal (anomalous) group velocity dispersion. Here, we focus on the case $s = -1$ and we supplement Eq. (1) with periodic boundary conditions $u(-L, t) = u(L, t)$, $t \geq 0$, $L > 0$, and initial condition $u(x, 0) = u_0(x)$, $\forall x \in \mathbb{R}$.

Variants of Eq. (1) appear in a variety of physical contexts, with the most prominent that of nonlinear optics [12]. In this case, t and x denote propagation distance and retarded time, respectively, while $u(x, t)$ is the electric field envelope. For ultra-short pulse propagation, third-order dispersion and self-steepening (characterized by coefficients β , μ and ν , respectively) become important, and corresponding versions of Eq. (1) find applications in nonlinear metamaterials [13] and water waves in finite depth [14–16]. Moreover, in the context of optics, and for relatively long propagation distances, dissipative effects, such as linear loss ($\gamma < 0$) [or gain ($\gamma > 0$)], as well as stimulated Raman scattering (SRS) of strength $\sigma_R > 0$, are also important [12]. Then, it is relevant to include nonlinear gain ($\delta > 0$) [or loss ($\delta < 0$)] to counterbalance the effects from the linear loss/gain mechanisms, which may potentially stabilize the solitons [17, 18].

As shown in Ref. [19], all possible regimes except $\gamma > 0$, $\delta < 0$, are associated with finite-time collapse or decay.

Furthermore, a critical value γ^* can be identified in the regime $\gamma < 0$, $\delta > 0$, which separates finite-time collapse from the decay of solutions. On the other hand, for $\gamma > 0$, $\delta < 0$, below we prove the existence of an attractor, and show numerically that it captures the full route from PB-type dynamics to quasi-periodic or chaotic dynamics.

The starting point of our proof is the power balance equation:

$$\frac{d}{dt} \int_{-L}^L |u|^2 dx = 2\gamma \int_{-L}^L |u|^2 dx + 2\delta \int_{-L}^L |u|^4 dx, \quad (2)$$

satisfied by any local solution $u \in C([0, T], H_{per}^k(\Omega))$, which initiates from sufficiently smooth initial data $u_0 \in H_{per}^k(\Omega)$, for fixed $k \geq 3$. Here, $H_{per}^k(\Omega)$ denotes the Sobolev spaces of periodic functions H_{per}^k [20], in the interval $\Omega = (-L, L)$. Analysis of (2), results in the asymptotic estimate: $\limsup_{t \rightarrow \infty} \frac{1}{2L} \int_{-L}^L |u(x, t)|^2 dx \leq -\frac{\gamma}{\delta}$, hence local in time solutions $u \in C([0, T], H_{per}^k(\Omega))$ are uniformly bounded in $L^2(\Omega)$. This allows for the definition of the extended dynamical system $\varphi(t, u_0) : H_{per}^k(\Omega) \rightarrow L^2(\Omega)$, $\varphi(t, u_0) = u$, whose orbits are bounded $\forall t \geq 0$. Moreover, from the above asymptotic estimate, we may derive, that if $L^2(\Omega)$ is endowed with the equivalent averaged norm $\|u\|_\alpha^2 = \frac{1}{2L} \int_{-L}^L |u|^2 dx$, its ball $\mathcal{B}_\alpha(0, \rho) = \{u \in L^2(\Omega) : \|u\|_\alpha^2 \leq \rho^2, \rho^2 > -\frac{\gamma}{\delta}\}$ attracts all bounded sets $\mathcal{B} \in H_{per}^k(\Omega)$. That is, there exists $T^* > 0$, such that $\varphi(t, \mathcal{B}) \subset \mathcal{B}_\alpha$, for all $t \geq T^*$. Thus, we may define for any bounded set $\mathcal{B} \in H_{per}^k(\Omega)$, $k \geq 3$, its ω -limit set in $L^2(\Omega)$, $\omega(\mathcal{B}) = \bigcap_{s \geq 0} \overline{\bigcup_{t \geq s} \varphi(t, \mathcal{B})}$. The closures are taken with respect to the weak topology of $L^2(\Omega)$. Then, the standard (embedding) properties of Sobolev spaces imply that the attractor $\omega(\mathcal{B})$ is at least weakly compact in $L^2(\Omega)$, or relatively compact in the dual space $H_{per}^{-1}(\Omega)$.

Next, the structure of the limit set $\omega(u_0)$, $u_0 \in \mathcal{B}$, is investigated by numerical integration via a high-accuracy pseudo-spectral method. With no loss of generality, we fix $\gamma = 1.5$, $\delta = -1$, $\mu = \nu = 0.01$, while third-order dispersion and SRS strengths, $\beta > 0$, $\sigma_R > 0$, are varied; additionally, the half length of Ω is fixed to $L = 50$. The phenomenology presented below is not significantly affected by the precise value of the relevant parameters. The limit set $\omega(u_0)$ is visualized by projections of the flow to suitable 2D or 3D spaces, defined by $\mathcal{P}_2 = \{(X, Y) \in \mathbb{R}^2\}$, and $\mathcal{P}_3 = \{(X, Y, Z) \in \mathbb{R}^3\}$. Here, $X(t) = |u(x_1, t)|^2$, $Y(t) = |u(x_2, t)|^2$, $Z(t) = |u(x_3, t)|^2$, for arbitrary spatial coordinates $x_1, x_2, x_3 \in \Omega$.

First, we use continuous wave (cw) initial data, $u_0(x) = \epsilon e^{-i \frac{K\pi x}{L}} \equiv \epsilon \phi_K$ of amplitude $\epsilon > 0$ and wave-number $K > 0$, which is an element of the 1D-linear subspace $\mathcal{V}_K = \{u \in L^2(\Omega) : u = \epsilon \phi_K(x), \epsilon > 0\}$ of $L^2(\Omega)$. Varying $\sigma_R > 0$, we find that $\omega(u_0)$ is an equilibrium state. Specifically, there exists a critical wave number K_{\max} such that: for $K < K_{\max}$, $\omega(u_0) = \phi_b$, i.e., a steady state of constant density $|\phi_b|^2 = -\frac{\gamma}{\delta}$, which attracts the cw initial data; for $K \geq K_{\max}$, $\omega(u_0) = \Phi_p$,

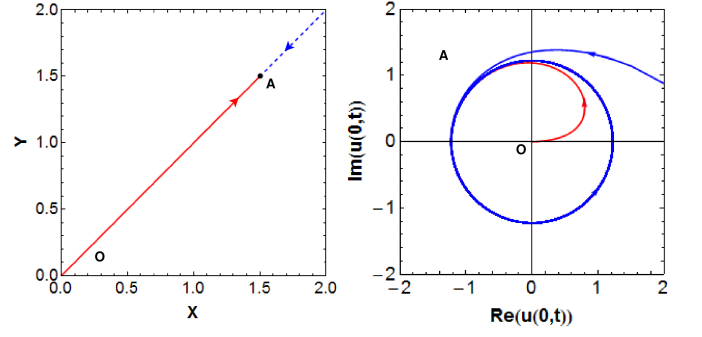


Figure 1: (Color Online) The scenario $\omega(u_0) = \{\phi_b\}$. Left panel: convergence to the fixed point **A**. Right Panel: the fixed point **A** as a limit circle of radius $\sqrt{-\gamma/\delta}$.

i.e., the dynamics is attracted to a steady state of spatially periodic density. In fact, the separatrix K_{\max} decreases as σ_R increases.

The dynamical scenario $\omega(u_0) = \{\phi_b\}$ for $\beta = 0.02$, $\sigma_R = 0.3$ and $K = 4 < K_{\max} = 5$ is illustrated in Fig. 1. The projection of the cw equilibrium ϕ_b to the 2D space \mathcal{P}_2 is the fixed point **A** $= (|\phi_b|^2, |\phi_b|^2) = (-\frac{\gamma}{\delta}, -\frac{\gamma}{\delta}) = (1.5, 1.5)$. The right panel of Fig. 1 illustrates the convergence of the projected linear orbits to **A**, associated to the choice of spatial coordinates $x_1 = 5, x_2 = 10$. The dashed blue (continuous red) line is the projection of the flow for the cw with $\epsilon = 3$ ($\epsilon = 0.01$); the arrows indicate the direction of the 2D-projection of the flow. The cw steady state ϕ_b is an element of \mathcal{V}_K , and only differs in amplitude from the initial condition. Hence, \mathcal{V}_K defines a stable linear subspace for **A**. The right panel of Fig. 1 visualizes the steady state ϕ_b as a limit circle **A** of radius $\sqrt{-\frac{\gamma}{\delta}} = \sqrt{1.5}$, in the 2D space $(\text{Re}(u(0, t)), \text{Im}(u(0, t)))$. The limit circle corresponds to the rotating linear oscillations of the real and imaginary parts of the solution u . Effectively in this case, the solution preserves its plane wave form but its amplitude, say, $h(t)$ satisfies $\dot{h} = \gamma h + \delta h^3$ and thus for $h(0) = \epsilon$, $\lim_{t \rightarrow \infty} h^2(t) = -\frac{\gamma}{\delta} \equiv |\phi_b|^2$.

Next, consider the scenario $\omega(u_0) = \{\Phi_p\}$, for $\beta = 0.02$, $\sigma_R = 0.3$, and $K = K_{\max} = 5$, illustrated in Fig. 2. The upper panel shows density snapshots for a cw-initial condition with $\epsilon = 0.01$. The solution has reached the cw-steady state ϕ_b exponentially fast, but at $t \approx 500$ the instability of the state ϕ_b emerges. Although transient oscillations of increasing amplitude occur (cf. snapshot at $t = 683$) due to the linear gain $\gamma > 0$, the nonlinear loss $\delta < 0$ prevents collapse of the solution. After $t \approx 685$, we observe convergence to the new steady state Φ_p (reached at $t \approx 700$), whose profile remains unchanged till the end of integration ($t = 3000$). The orbital connection, via the transient dynamics, between steady states ϕ_b and Φ_p is illustrated in the projections of the flow on the spaces \mathcal{P}_2 and \mathcal{P}_3 – cf. bottom left and right panels of Fig. 2, respectively, for $x_1 = 0$ and $x_2 = 4.5$. In 2D, **B** $\approx (1.5, 0.15)$ is the new fixed point, while in 3D, **A** $= (1.5, 1.5, 1.5)$ and **B** $\approx (1.5, 0.15, 1.16)$. The infinite-dimensional orbital

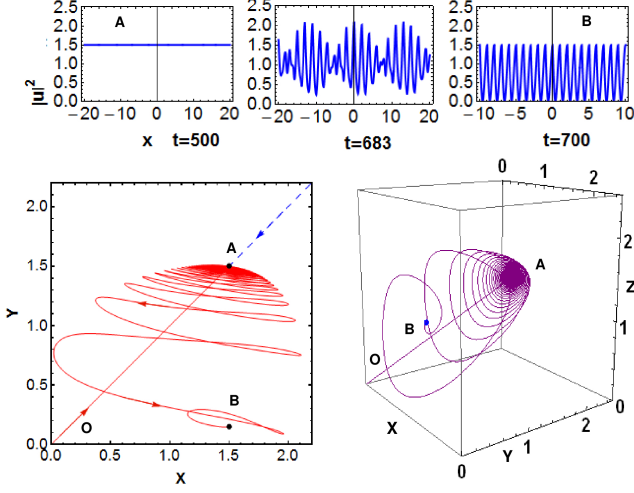


Figure 2: (Color Online) The scenario $\omega(u_0) = \{\Phi_p\}$. Upper panels: density snapshots. Bottom panels: orbital connections $O \rightarrow A \rightarrow B$ in 2D (left) and 3D (right) spaces.

connection $\{0\}$ (unstable) $\xrightarrow{\mathcal{O}_1} \{\phi_b\}$ (unstable) $\xrightarrow{\mathcal{O}_2} \{\Phi_p\} = \omega(u_0)$, where \mathcal{O}_1 and \mathcal{O}_2 denote the orbits connecting the steady states, is projected to the 2D and 3D-connections O (unstable) $\xrightarrow{\mathcal{O}'_1} \{A\}$ (unstable) $\xrightarrow{\mathcal{O}'_2} \{B\}$. The projected orbits highlight the spiraling of the stable manifold of the limit point B around the unstable linear subspace of $O = (0, 0, 0)$ connecting O and A . The connection was found to be stable with respect to variations of ϵ – cf. linear dashed blue (continuous red) converging orbit in the bottom left panel, corresponding to a cw-initial condition of amplitude $\epsilon = 2$ ($\epsilon = 0.01$).

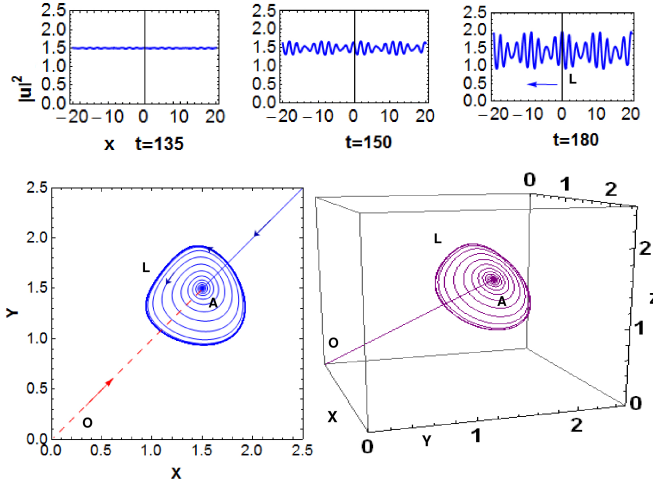


Figure 3: (Color Online) The dynamics scenario $\omega(u_0) = L$, i.e., a space-time periodic traveling wave. Upper panels: density snapshots. Bottom panels: convergence $O \rightarrow A \rightarrow L$, the limit cycle in 2D (left) and 3D (right) spaces.

Increasing β , for $\sigma_R = 0.01$, we observe the birth of yet another feature, namely traveling space-time oscilla-

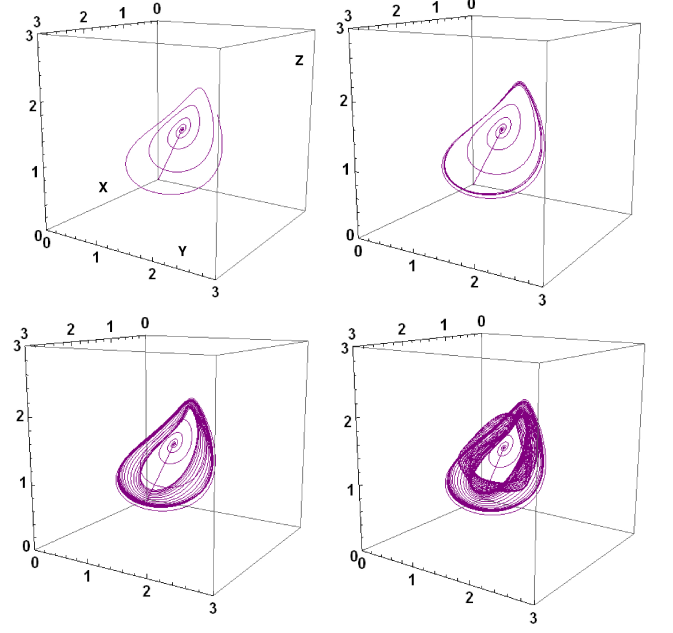


Figure 4: (Color Online) Birth of a chaotic attractor $\omega(u_0) = S$. Transition from the instability of the cw-steady state A , to quasiperiodic, and to chaotic behavior for $t \in [0, 350]$.

tions. Upper panel of Fig. 3 shows density snapshots, for a cw initial condition of $K = 5$, $\epsilon = 0.01$, and $\beta = 0.55$. Now, instability of the steady-state ϕ_b , leads to the birth of a stable, traveling space-time periodic solution, whose profile is shown for $t = 180$ (arrow indicates propagation direction). The projections, for $x_1 = 0$, $x_2 = 5$ and $x_3 = 10$, on \mathcal{P}_2 (bottom left panel) and \mathcal{P}_3 (bottom right panel), visualize the periodic solution as a limit cycle L , i.e., a periodic orbit. The continuous blue (dashed red) linear orbit shown in the bottom left panel, corresponds to the cw-initial condition of $K = 5$ and $\epsilon = 3$ ($\epsilon = 0.01$), highlighting the stability (i.e., attracting nature) of the limit cycle with respect to ϵ . Third-order dispersion plays a critical role in this scenario of $\omega(u_0) = L$. Specifically, for fixed $\sigma_R = 0.01$ and $K > 4$, there exists an interval $I_{\beta,K} = [\beta_{\min}(K), \beta_{\max}(K)]$, such that for some $\beta \in I_{\beta,K}$, the initial condition may converge to a space-time periodic solution; e.g., for $K = 5$, $I_{\beta,5} \approx [0.5, 0.57]$, while for $K = 20$, $I_{\beta,20} \approx [0.7, 1.2]$. On the other hand, when $\beta \notin I_{\beta,K}$, the initial condition converges to a steady state. Evidently, the structure of the limit set $\omega(u_0)$ for Eq. (1), consisting either of distinct equilibria and orbits connecting them, or being a limit cycle, is reminiscent of scenarios associated with PB dynamics.

The interval $I_{\beta,K}$ may be partitioned to sub-intervals where quasi-periodic, or even chaotic behavior emerges. Figure 4 shows the 3D-projection of the flow on \mathcal{P}_3 , for $x_1 = 5$, $x_2 = 10$, $x_3 = 15$, $t \in [0, 350]$, $\beta = 0.52$, $\sigma_R = \mu = \nu = 0.01$, for a cw of $\epsilon = 0.01$ and $K = 5$. We observe the birth of quasi-periodic orbits from the instability of the steady-state ϕ_b , and the transition to chaotic

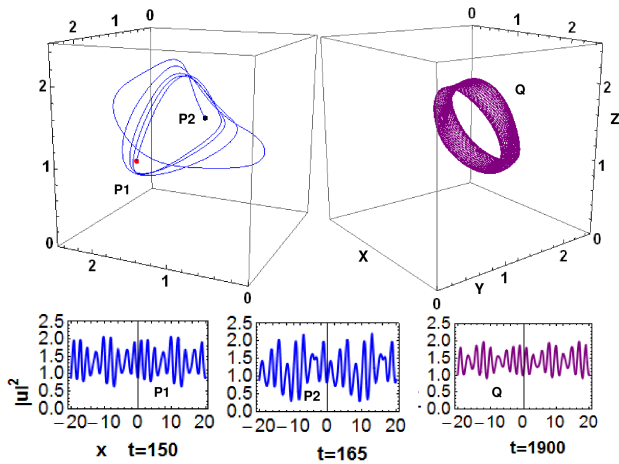


Figure 5: (Color Online) Top left panel: a chaotic path in \mathbf{S} for $t \in [180, 200]$. Top right panel: projection in 3D-space \mathcal{P}_3 of the invariant torus-like set \mathbf{Q} for $t \in [1800, 2000]$. Bottom panels: chaotic waveforms, corresponding to points $\mathbf{P1}$ (left) and $\mathbf{P2}$ (middle), and a quasi-periodic solution in \mathbf{Q} (right).

behavior manifested by their trapping to a chaotic attractor \mathbf{S} .

The upper left panel of Fig. 5 shows part of a chaotic orbit in \mathbf{S} , for $t \in [180, 200]$, and $\beta = 0.5 \approx \beta_{\min}(5)$. The first two snapshots of the bottom panel show profiles of the solution corresponding to points $\mathbf{P1}$ and $\mathbf{P2}$, for $t = 150$ and $t = 165$. The “windings” of the chaotic orbits are evident in the upper left panel of Fig. 5, similarly also to the bottom right panel of Fig. 4. The chaotic behavior manifests itself in the time-fluctuating amplitude, the changes in the waveform’s spatial periodicity, and in the propagation direction of the chaotic traveling wave.

The interval $I_{\beta,K} = [\beta_{\min}(K), \beta_{\max}(K)]$ can be partitioned in the following sub-intervals: a chaotic $I_{\beta,K,c} = [\beta_{\min}(K), \beta_{\text{ch}}(K)]$, a quasi-periodic $I_{\beta,K,q} = (\beta_{\text{ch}}(K), \beta_{\text{lc}}(K))$, and a limit-cycle one $I_{\beta,K,lc} = [\beta_{\text{lc}}(K), \beta_{\max}(K)]$. Let $\beta_{\min}(K)$ be the critical value for

the onset of the quasiperiodic behavior and the transition to the chaotic regime. Then, as $\beta \rightarrow \beta_{\text{ch}}(K)$, the chaotic behavior weakens, and chaotic solutions emerge at later times. Chaotic orbits still exist for $\beta = \beta_{\text{ch}}(K)$. For $\beta > \beta_{\text{ch}}(K)$, solutions remain quasi-periodic, and the orbit is trapped within an invariant torus-like set \mathbf{Q} . For $K = 5$, we find that $\beta_{\text{ch}}(5) \approx 0.53$. The projection on \mathcal{P}_3 of \mathbf{Q} for $\beta = 0.54 > \beta_{\text{ch}}(5)$, is shown in the upper right panel of Fig. 5. The orbit is plotted for $t \in [1800, 2000]$, and the profile of a quasi-periodic solution within \mathbf{Q} at $t = 1900$ is shown in the third snapshot of the bottom panel. The set \mathbf{Q} persists as long as $\beta < \beta_{\text{cl}}(K)$. When $\beta_{\text{lc}}(K) \leq \beta \leq \beta_{\max}(K)$, the set \mathbf{Q} is replaced by a limit cycle. For $K = 5$, we find the following sub-intervals of $I_{\beta,5} \approx [0.5, 0.57]$: the chaotic $I_{\beta,5,c} \approx [0.5, 0.53]$, the quasi-periodic $I_{\beta,5,q} \approx (0.53, 0.55)$, and the limit-cycle $I_{\beta,5,lc} \approx [0.55, 0.57]$. For $K = 5$, the above sub-intervals were detected with accuracy 10^{-3} : for $\beta = 0.549$, the set \mathbf{Q} persists, while for $\beta = 0.55$, the initial state is trapped on the limit cycle.

In conclusion, we have revealed that the infinite-dimensional dynamics of a physically important and broadly relevant higher-order NLS model can be reduced in a wide parametric range to a sequence of low-dimensional dynamical scenarios (fixed points, periodic and quasi-periodic, as well as chaotic orbits) that can be suitably revealed in reduced (two- and three-dimensional) phase space representations. In particular, the competition between third-order dispersion and SRS effect, trace a path from Poincaré-Bendixson – type behavior to quasi-periodic or chaotic dynamics. These dynamical transitions are also reminiscent of ones observed in the path towards optical turbulence phenomena [22]. Our results suggest further investigations, including the identification of a low-dimensional attractor, its dimension and dependence on the spatial length [9], and the construction of the appropriate finite-dimensional reduced systems able to capture the effective low dimensional dynamics [23].

-
- [1] M. J. Ablowitz and H. Segur, *Solitons and Inverse Scattering Transform* (SIAM, 1981).
 - [2] Yu.S. Kivshar and G.P. Agrawal, *Optical solitons: from fibers to photonic crystals*, Academic Press (San Diego, 2003).
 - [3] D. Sanvitto, V. Timofeev, *Exciton polaritons in microcavities*, Springer-Verlag (Berlin, 2012).
 - [4] M. W. Hirsch, S. Smale, and R. L. Devaney, *Differential equations, dynamical systems, and an introduction to chaos*, Elsevier, 2004.
 - [5] I. G. Kevrekidis, B. Nicolaenko, and J. C. Scovel, *SIAM J. Appl. Math.* **50**, 760 (1990); F. Christiansen, P. Cvitanović, V. Putkaradze, *Nonlinearity* **10**, 55 (1997).
 - [6] K. Nozaki, N. Bekki, *Phys. Rev. Lett.* **51**, 2171 (1983); R. J. Deissler, H. R. Brand, *Phys. Rev. Lett.* **72**, 478 (1994).
 - [7] K. Nozaki, N. Bekki, *Phys. Rev. Lett.* **50**, 1226 (1983); *Physica D* **21**, 381 (1986); *Phys. Lett. A* **102**, 383 (1984);
 - [8] D. Cai, D. W. McLaughlin, and J. Shatah, *Phys. Lett. A* **253**, 280 (1999).
 - [9] E. Shlizerman and V. Rom-Kedar, *Chaos* **15**, 013107 (2005); see also: *Phys. Rev. Lett.* **96**, 024104 (2006) and *Phys. Rev. Lett.* **102**, 033901 (2009).
 - [10] Y. Li and D. W. McLaughlin, *Commun. Math. Phys.* **162**, 175 (1994); G. Haller and S. Wiggins, *Phys. D* **85**, 311 (1995);
 - [11] A. R. Bishop, K. Fesser, P. S. Lomdahl, W. C. Kerr, M. B. Williams, and S. E. Trullinger, *Phys. Rev. Lett.* **50**, 1095 (1983); A. R. Bishop, M. G. Forest, D. W. McLaughlin, E. A. Overman II, *Phys. Lett. A*, **144**, 17 (1990); G. Kovačič and S. Wiggins, *Physica D* **57**, 185

- (1992); N. Ercolani, M. G. Forest, D. W. McLaughlin, *Physica D* **43**, 349 (1990).
- [12] A. Hasegawa and Y. Kodama, *Solitons in optical communications*, Oxford University Press, 1996; G. P. Agrawal, *Nonlinear Fiber Optics*, Academic Press, 2012; Yu. S. Kivshar and G. P. Agrawal, *Optical Solitons: From Fibers to Photonic Crystals*, Academic Press, 2003.
- [13] M. Scalora, M. S. Syrchin, N. Akozbek, E. Y. Poliakov, G. D'Aguzzo, N. Mattiucci, M. J. Bloemer, and A. M. Zheltikov, *Phys. Rev. Lett.* **95**, 013902 (2005); S. Wen, Y. Xiang, X. Dai, Z. Tang, W. Su, and D. Fan, *Phys. Rev. A* **75**, 033815 (2007); N. L. Tsitsas, N. Rompotis, I. Kourakis, P. G. Kevrekidis, and D. J. Frantzeskakis, *Phys. Rev. E* **79**, 037601 (2009).
- [14] R. S. Johnson, *Proc. R. Soc. Lond. A* **357**, 131 (1977).
- [15] Yu. V. Sedletsky, *J. Exp. Theor. Phys.* **97**, 180 (2003).
- [16] A. V. Slunyaev, *J. Exp. Theor. Phys.* **101**, 926 (2005).
- [17] H. Ikeda, M. Matsumoto, and A. Hasegawa, *Opt. Lett.* **20** (1995), 1113.
- [18] T. P. Horikis and D. J. Frantzeskakis, *Opt. Lett.* **38**, 5098 (2013).
- [19] V. Achilleos, S. Diamantidis, D. J. Frantzeskakis, T. P. Horikis, N. I. Karachalios, and P. G. Kevrekidis, *arXiv:1505.04378*.
- [20] R. Temam, *Infinite-Dimensional Dynamical Systems in Mechanics and Physics*, Springer-Verlag, 1997.
- [21] D. J. Frantzeskakis, *J. Phys. A* **29**, 3631 (1996).
- [22] K. Ikeda, H. Daido, O. Akimoto, *Phys. Rev. Lett.* **45**, 709 (1980).
- [23] P. Cvitanović, R. L. Davidchack, and E. Siminos, *SIAM J. Appl. Dyn. Syst.* **9**, 1 (2010).